Analysis of discrete adjoint fields for 2D Euler flows

Jacques Peter, Clément Labbé, Florent Renac

Analysis of discrete adjoint fields for 2D Euler flows

Jacques Peter*, Clément Labbé, Florent Renac
ONERA/DAAA
22 av de la Division Leclerc, 92322 Châtillon Cedex, France
Email: jacques.peter@onera.fr, clement.labbe@onera.fr, florent.renac@onera.fr

Summary
Discrete and continuous adjoint are well established methods to efficiently calculate derivatives of aerodynamic functions with respect to numerous design parameters. Whereas very accurate adjoint codes have been developped for complex models as soon as end of 90's,[1,2] a number of questions relative to the solutions of discrete and continuous adjoint fields are still open, even for inviscid flows. We first compute discrete lift and drag adjoint fields on a hierarchy of meshes that includes very fine meshes. After it has been checked that they more and more closely satisfy the continuous equation (by discretizing all corresponding terms at cell centers), we discuss the continuous adjoint boundary conditions and the explicit analytic relation of Pierce and Giles.[3] For a supersonic flow case, the consistency of the adjoint fields upwind the detached shock-wave with a simple wave decomposition is also explored. Besides, the physical residual perturbation method[3] is used to understand the location of the areas exhibiting strong adjoint values.

Keywords: *discrete adjoint, continuous adjoint, dual consistency, 2D flow, inviscid flow*

1 Introduction

Discrete and continuous adjoint methods are now well established[4] and adjoint-based derivatives are commonly used for local shape optimization and also in other fields like metamodeling, uncertainty-quantification or stability analysis. Concerning discrete adjoint, it is to be noted that strong efforts have been devoted to code (either by hand or using automatic differentiation) the exact linearization of complex schemes for complex models[1,2] whereas fundamental questions relative to discrete adjoint fields are still open : are they consistent with the continuous equation at the limit of fine meshes ? This is unknown for finite volume schemes except for specific cases and schemes.[5–7] What is the asymptotic behaviour of lift and drag adjoint fields at stagnation streamline ? It seems that the law predicted by Giles and Pierce for inviscid flows (inverse of distance-to-line square root) is not always clearly observed (see for example[8,9] for an example with continuous adjoint fields). Under what conditions increasingly high values of lift and drag adjoint are observed at the wall for inviscid flows, in particular at the trailing edge ?

To contribute to the understanding of these issues, lift and drag adjoint fields are computed about the NACA0012 for four flow conditions (M_∞,AoA)=(0.4,5^o), (0.85,2^o), (0.95,0^o) and (1.5,1^o) previoulsy retained in many publications. The flow and adjoint calculations are run on the series of very regular meshes used by Vassberg and Jameson in a classical article.[10] These structured meshes exhibit high regularity and orthogonal lines. Their far-field boundary is located at about 150 chords to the profile. They are hence well-adapted for accurate finite volume discretization and for mesh convergence studies of lifting and non-lifting flows. The five meshes ranging from (129×129) to (2049× 2049) nodes are considered and calculations are run with the Jameson-Schmidt-Turkel scheme using the *elsA* code.[11] (Note that *elsA* is a cell-centered Finite-Volume code, so that the location of the adjoint variables for the last row of cell adjacent to a boundary is not fixed as the mesh is refined.)
The terms of the continuous adjoint equations are then calculated at cell-centers for the discrete adjoint fields and it is checked that this equation is more and more closely satisfied as the mesh is refined. The consistency of the finest-grid lift and drag adjoint with the other properties that they are expected to satisfy – wall boundary condition, far-field boundary condition, property demonstrated by Giles and Pierce – are then discussed as well as specific properties depending on the flow conditions.

2 Reminder about continuous adjoint for 2D Euler flows

The continuous adjoint equations for compressible flows were first derived by Jameson:[12] in the case of a 2D Euler flow about a profile, he considered a body fitted structured grid that was mapped to a fixed (ξ, η) rectangle. The Euler equations in these (ξ, η) coordinates were used. A parametrization of the mapping then allowed to vary the airfoil shape in the physical space (without altering the domain of variation of the transformed coordinates) and to

define a gradient calculation problem for functional outputs. The adjoint method was also well described by Giles and Pierce[13,14] in this framework.

As, in this formulation, the system of transformed coordinates is attached to a structured mesh, the aforementioned equations could not be used for unstructured CFD for which a formulation in physical coordinates was necessary. The corresponding system of equations was first published by Anderson and Venkatakrishnan in 1998[15] (and one year later by Hiernaux and Essers[16,17]). A slightly simplified presentation of the theoretical part of reference[15] is given below.

The quantity of interest is assumed to be the projection of the force applied by the fluid onto the solid, projected in direction $\overline{d}$ (in practice, lift or drag):

$$J = \left(\int_{\Gamma_w} p\overline{n} ds \right) .\overline{d} = \int_{\Gamma_w} p(\overline{n}.\overline{d}) ds,$$

where Γ_w is the boundary of the solid body, $\overline{n}$ is the local normal (external for fluid and internal for the solid) and p is the static pressure at a boundary point. The 2D Euler equations are denoted

$$\frac{\partial F_x(W)}{\partial x} + \frac{\partial F_Y(W)}{\partial y} = 0,$$

W being the conservative variables and F_x and F_Y the classical fluxes of convervative form of Euler equations,

$$F_X = \begin{pmatrix} \rho u \\ \rho u_x^2 + p \\ \rho u_x u_y \\ \rho u_x H \end{pmatrix} \quad F_Y = \begin{pmatrix} \rho u_y \\ \rho u_x u_y \\ \rho u_y^2 + p \\ \rho u_y H \end{pmatrix}.$$

Let us note δW the pertubation in the steady state flow that is caused be an infinitesimal pertubation of airfoil shape or flow conditions. As W and $W + \delta W$ are solutions of steady Euler equations for initial and perturbed problem, by difference

$$\frac{\partial (A\delta W)}{\partial x} + \frac{\partial (B\delta W)}{\partial y} = 0,$$

(A and B being the Jacobian of Euler fluxes F_x and F_Y). The perturbation in J value can be augmented by the dot product of last equation by an arbitrary co-state field ψ

$$\delta J = \int_{\Gamma_w} \delta p(\overline{n}.\overline{d}) ds + \int_{\Gamma_w} p(\delta(\overline{n}).\overline{d}) ds + \int_{\Gamma_w} p(\overline{n}.\overline{d}) \delta(ds) + \int_{\Omega} \psi^T \left(\frac{\partial (A\delta W)}{\partial x} + \frac{\partial (B\delta W)}{\partial y} \right) dv.$$

The last term can be transformed by integration by parts into

$$- \int_{\Omega} \left(\frac{\partial \psi^T}{\partial x} A + \frac{\partial \psi^T}{\partial x} B \right) \delta W dv + \int_{\Gamma_w} \psi^T (An_x + Bn_y) \delta W ds + \int_{\Gamma_\infty} \psi^T (An_x + Bn_y) \delta W ds.$$

For any regular ψ function, the pertubation in the objective may then be rewritten

$$\delta J = \int_{\Gamma_w} \delta p(\overline{n}.\overline{d}) ds + \int_{\Gamma_w} p(\delta(\overline{n}).\overline{d}) ds + \int_{\Gamma_w} p(\overline{n}.\overline{d}) \delta(ds) - \int_{\Omega} \left(\frac{\partial \psi^T}{\partial x} A + \frac{\partial \psi^T}{\partial x} B \right) \delta W dv + \int_{\Gamma_w} \psi^T (An_x + Bn_y) \delta W ds + \int_{\Gamma_\infty} \psi^T (An_x + Bn_y) \delta W ds. \quad (1)$$

The adjoint method removes the dependancy in the flow perturbation δW for the calculation of the variation of one specific objective J. This directly yields the adjoint equation in the fluid domain

$$-A^T \frac{\partial \Psi}{\partial x} - B^T \frac{\partial \Psi}{\partial y} = 0. \quad (2)$$

Besides the wall boundary conditions links $\delta\overline{n}$ and δW:

$$\delta(\overline{V}.\overline{n}) = \delta(\overline{V}).\overline{n} + \overline{V}.\delta(\overline{n}) = 0$$

so that the second and third components of δW satisfy

$$\delta W_2 \; n_x + \delta W_3 \; n_y + W_2 \; \delta n_x + W_3 \; \delta n_y = 0 \quad (3)$$

The explicit calculation of $\psi^T (An_x + Bn_y) \delta W$ at the wall yields

$$\psi^T (An_x + Bn_y) \delta W = (n_x \psi_2 + n_y \psi_3) \times \left((\gamma - 1) \frac{V^2}{2}, (1-\gamma)u, (1-\gamma)v, (\gamma - 1) \right) \begin{pmatrix} \delta W_1 \\ \delta W_2 \\ \delta W_3 \\ \delta W_4 \end{pmatrix} + (\psi_1 + u\psi_2 + v\psi_3 + H\psi_4)(n_x \delta W_2 + n_y \delta W_3)$$

The last term is reformulated using the linearized boundary condition (3), then the sum of the terms involving the flow variation δW in the integrals over Γ_w is set to zero to define the adjoint wall boundary condition,

$$\frac{dp}{dW}(\overline{n}.\overline{d}) + (n_x \psi_2 + n_y \psi_3) \times \left((\gamma - 1) \frac{V^2}{2}, (1-\gamma)u, (1-\gamma)v, (\gamma - 1) \right) \begin{pmatrix} \delta W_1 \\ \delta W_2 \\ \delta W_3 \\ \delta W_4 \end{pmatrix} = 0. \quad (4)$$

The dot product in the last term of (4) corresponds to the derivative of the static pressure with respect to the conservative variables, so that the final and classical form of the boundary condition is simply

$$\overline{n}.\overline{d} + \Psi_2 n_x + \Psi_3 n_y = 0. \quad (5)$$

In the farfield, no variation of the boundary needs to be considered. The Jacobian in direction (n_x, n_y) can be

rewritten by using a locally one dimensionnal characteritic decompostion to yield

$$\int_{\Gamma_\infty} \psi^T (An_x + Bn_y)\delta W ds = \int_{\Gamma_\infty} (\psi^T P^{-1} DP\delta W) ds. \quad (6)$$

It is assumed that $P\delta W \simeq \delta(PW)$. The variation in these characteristic variables is zero for the components corresponding to negative eigenvalues of the Jacobian, $An_x + Bn_y$, in the classical 1D approximate linearization at the boundary (information coming from outside of the domain and fixed characteristic value). The far-field adjoint BC simply imposes that the other components of $\psi^T P^{-1}$ are zero so that the line-vector times diagonal-matrix times column-vector, $\psi^T P^{-1} \times D \times P\delta W$, is zero.

3 Reminder about discrete adjoint

3.1 Discrete gradient calculation

The finite volume scheme of interest defines the steady-state discrete flow W (size n_W) as the solution of a set of n_W non linear equations involving W and the mesh coordinates, denoted X,

$$R(W,X) = 0.$$

If the volume mesh is a regular function of a vector of design parameters α (size n_α), under classical mathematical assumptions,[4] the implicit implicit function theorem allows to define W as a function of (X and then of) α. Discrete gradient calculation consists in computing the derivatives of n_f functions

$$\mathscr{J}_k(\alpha) = \mathrm{J}_k(W(\alpha), X(\alpha)) \qquad k \in \{1...n_f\}$$

with respect to the n_α design parameters. Most often, at least for external aerodynamics, n_α is much larger than n_f and the most efficient way to proceed is to use the discrete adjoint equation,

$$\left(\frac{\partial R}{\partial W}\right)^T \Lambda_k = -\left(\frac{\partial \mathrm{J}_k}{\partial W}\right)^T, \quad (7)$$

then calculate

$$\frac{\mathrm{d}\mathscr{J}_k(\alpha)}{\mathrm{d}\alpha} = \frac{\partial \mathrm{J}_k}{\partial X}\frac{\mathrm{d}X}{\mathrm{d}\alpha} + \Lambda_k^T \left(\frac{\partial R}{\partial X}\frac{\mathrm{d}X}{\mathrm{d}\alpha}\right).$$

The dominant cost is the inversion of the n_f linear systems of size n_W whereas all other classical methods solve n_α linear (or possibly non-linear) systems of size n_W.

3.2 Numerical characterization of discrete ajoint

It is classical to identify the adjoint vector Λ of one of the functions, J, to the sensitivity of this function to a perturbation of residual R followed by reconvergence: let $W + \delta W$ be the new converged flow corresponding to pertubed residual $R + \delta R$. Obviously

$$(R + \delta R)(W + \delta W, X) = 0,$$

or at first order

$$\delta R + \frac{\partial R}{\partial W}\delta W = 0$$

The first order change in the function of interest J due to change in flow δW is

$$\delta \mathrm{J} = -\frac{\partial \mathrm{J}}{\partial W}\left(\frac{\partial R}{\partial W}\right)^{-1}\delta R$$

since

$$\mathrm{J}(W + \delta W, X) \simeq \mathrm{J}(W,X) + \left(\frac{\partial \mathrm{J}}{\partial W}\right)\delta W.$$

Involving discrete adjoint vector Λ, yields

$$\delta \mathrm{J} = \Lambda^T \delta R \quad (8)$$

If only the a-th component of R at cell index m has been arbitrarly altered by a small number δR_m^a, then previous equation yields

$$\Lambda_m^a = \delta \mathrm{J} / \delta R_m^a. \quad (9)$$

This defines the a-th component of Λ at cell index m as the limit ratio of change in J divided by the infinitesimal change in the residual R at the corresponding cell & component which caused the change in the flow and the function value.

3.3 Physical characterization of adjoint for 2D Euler flows

Up to that point, the adjoint vector appears as a mathematical object, dual of the residual R, and there is no reason to expect mesh convergence and consistency with continuous adjoint except for specific discretizations[5–7] that have been proved to be dual consistent. However, in a well-known conference paper, Giles and Pierce proposed a physical point of view[3] for 2D inviscid flows. Four physical source terms δR are defined at each individual cell (this location when transposing their idea from continuous to discrete adjoint): (1) local mass source at fixed stagnation pressure and total enthalpy ; (2) local normal force ; (3) local change in total enthalpy at fixed static and total pressure ; (4) local change in total pressure at fixed total enthalpy and static pressure.

$$\delta R_m^1 = \varepsilon \begin{pmatrix} 1 \\ u_x \\ u_y \\ H \end{pmatrix} \quad \delta R_m^2 = \varepsilon \begin{pmatrix} 0 \\ -\rho u_y \\ \rho u_x \\ 0 \end{pmatrix}$$

$$\delta R_m^3 = \varepsilon \begin{pmatrix} -\frac{1}{2H} \\ 0 \\ 0 \\ \frac{1}{2} \end{pmatrix} \quad \delta R_m^4 = \varepsilon \begin{pmatrix} \frac{1}{p_0}\left(\frac{\gamma-1}{\gamma} + \frac{1}{\gamma M^2}\right) \\ \frac{u_x}{p_0}\left(\frac{\gamma-1}{\gamma} + \frac{2}{\gamma M^2}\right) \\ \frac{u_y}{p_0}\left(\frac{\gamma-1}{\gamma} + \frac{2}{\gamma M^2}\right) \\ \frac{H}{p_0}\left(\frac{\gamma-1}{\gamma} + \frac{1}{\gamma M^2}\right) \end{pmatrix}$$

(using the usual notation of aerodynamics). By the mean of mechanical analysis, the corresponding function variations $\delta J^{(1m)}$, $\delta J^{(2m)}$, $\delta J^{(3m)}$, $\delta J^{(4m)}$ due to the source terms in

cell m, δR^1_m, δR^2_m, δR^3_m and δR^4_m, are supposed to be exactly calculated and (assuming they are exact)

$$(\delta \mathrm{J}^{(1m)}, \delta \mathrm{J}^{(2m)}, \delta \mathrm{J}^{(3m)}, \delta \mathrm{J}^{(4m)}) = (\Lambda_{1,m}, \Lambda_{2,m}, \Lambda_{3,m}, \Lambda_{4,m}) \times \begin{pmatrix} \delta R^1_{1,m} & \delta R^2_{1,m} & \delta R^3_{1,m} & \delta R^4_{1,m} \\ \delta R^1_{2,m} & \delta R^2_{2,m} & \delta R^3_{2,m} & \delta R^4_{2,m} \\ \delta R^1_{3,m} & \delta R^2_{3,m} & \delta R^3_{3,m} & \delta R^4_{3,m} \\ \delta R^1_{4,m} & \delta R^2_{4,m} & \delta R^3_{4,m} & \delta R^4_{4,m} \end{pmatrix}$$

where the (dm) superscript for $\delta \mathrm{J}$ means change in J function due to d-th change of R at cell m, reconverging flow W with global change δW^d which leads to the change $\delta \mathrm{J}^{(dm)}$ of the function of interest. As the four changes in R are linearly independent, Giles and Pierce may define the adjoint vector at cell m as

$$(\Lambda^1_m, \Lambda^2_m, \Lambda^3_m, \Lambda^4_m) = (\delta \mathrm{J}^{(1m)}, \delta \mathrm{J}^{(2m)}, \delta \mathrm{J}^{(3m)}, \delta \mathrm{J}^{(4m)}) \times \begin{pmatrix} \delta R^1_{1,m} & \delta R^2_{1,m} & \delta R^3_{1,m} & \delta R^4_{1,m} \\ \delta R^1_{2,m} & \delta R^2_{2,m} & \delta R^3_{2,m} & \delta R^4_{2,m} \\ \delta R^1_{3,m} & \delta R^2_{3,m} & \delta R^3_{3,m} & \delta R^4_{3,m} \\ \delta R^1_{4,m} & \delta R^2_{4,m} & \delta R^3_{4,m} & \delta R^4_{4,m} \end{pmatrix}^{-1}$$

where the inverse matrix in equation (10) can be explicited using formal calculation. It reads

$$\frac{1}{\varepsilon} \begin{pmatrix} -1 - \frac{(\gamma-1)}{2} M^2 & -\frac{(1+(\gamma-1)M^2)u}{V^2} & -\frac{(1+(\gamma-1)M^2)w}{V^2} & \frac{1+\frac{(\gamma-1)}{2}M^2}{H} \\ 0 & -\frac{w}{\rho V^2} & \frac{u}{\rho V^2} & 0 \\ -H & 0 & 0 & 1 \\ -\frac{p_0 \gamma M^2}{2} & \frac{p_0 \gamma u}{c^2} & \frac{p_0 \gamma w}{c^2} & -\frac{p_0 \gamma M^2}{2H} \end{pmatrix} \quad (10)$$

This of course is derived from (8) and close to it, except that the residual perturbations δR have been physically defined which makes the local discrete adjoint vector physically defined. For all systems of equation for which a similar demonstration can be done, the adjoint vector gets intrinsic and we can expect similar solutions from different discretizations and also mesh convergence. Let us finally note that not only the Λ components can be plotted, as usually done but also, in the spirit of Giles and Pierce, the limit ratio of the $\delta \mathrm{J}^{(d)}$ divided by ε (the small parameter of the physical source term).

Finally, Giles and Pierce have noted that perturbation δR^3 does not alter the pressure field for inviscid flows. It has hence no influence on drag and lift for which

$$\delta \mathrm{J} = 0 = \Lambda \delta R^3 = \Lambda_1 - H \Lambda_4.$$

This leads to the only first integral of adjoint field we are aware of: For functions of the pressure only and inviscid flows

$$\Lambda_1 = H \Lambda_4 \quad (11)$$

This property is actually well satisfied by numerical discrete adjoint fields. In the plots presenting the drag and lift adjoints (figure 15 and 16) the Λ_4 selected iso-values are defined as those of Λ_1 divided by the far-field total enthalpy H_∞ (that, of course, should be the local value all over the fluid domain for these Euler flows). These plots hence allow to check that the theoretical equation (11) is almost perfectly satisfied by the numerical adjoint fields.

3.4 Behavior of discrete adjoint at the wall

This question is discussed for a cell-centred finite-volume code like the *elsA* code of ONERA.[11] Using the cell-centred approach, in the direct steady-state mode, a boundary state W_b is derived from the adjacent conservative variables W for each boundary interface ; W_b satisfies all Dirichlet like relations to be imposed at the boundary. In the discrete adjoint mode, the adjoint variables are associated to cell-centred residual so that there is no adjoint variable located at the interface boundaries. Nevertheless, it is possible to write specifically the discrete adjoint equation of a cell adjacent to a wall-boundary (at cell of indices (i,1), see figure 1)

$$\sum_k \Lambda^T_k \frac{\partial R_k}{\partial W_{(i,1)}} = -\frac{\partial J}{\partial W_{(i,1)}} \quad (12)$$

and search for the dominant terms.

Near-field aerodynamic functions like pressure lift or drag are calculated based on wall-interface conservative variables, W_b. In the framework of the *elsA* code, specific ONERA post-processing codes calculate near field and far-field functions J and their derivatives $(\partial J/\partial W)$, $(\partial J/\partial W_b)$ and $(\partial J/\partial X)$ whereas the *elsA* code calculates the boundary condition Jacobian $(\partial W_b/\partial W)$. The exact form of right-hand side of previous equation for a near-field function is hence (for a cell of indices $(i,1)$, adjacent to the wall)

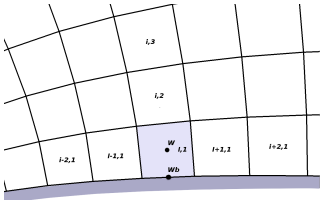

Figure 1: state variable W and boundary variable W_b

$$-\frac{\partial J}{\partial W_{b_{(i,1/2)}}} \frac{\partial W_{b_{(i,1/2)}}}{\partial W_{(i,1)}}$$

[1] The considered numerical fluxes, which balance is equal to the residual R, are four-point second order formula for ordinary interfaces, namely Jameson et al. flux[18] or Roe flux with MUSCL approach and van Albada limiting function.[19–21] At the solid wall (indices $(1/2, j)$) or far-field, the numerical flux is the physical flux of the W_b boundary state. At the next face (indices $(3/2, j)$) the standard flux formula is applied involving a ghost cell (indices $(i,0)$) where the state variables are set to $2W_{b(i,1/2)} - W_{(i,1)}$. For this type of scheme equation (12)

[1] Metric terms are involed in most boundary conditions formula so that partial derivatives is more rigorous.

reads

$$(\Lambda^T_{(i-2,1)}-\Lambda^T_{(i-1,1)})\frac{\partial F_{i-3/2,1}}{\partial W_{(i,1)}}+(\Lambda^T_{(i-1,1)}-\Lambda^T_{(i,1)})\frac{\partial F_{i-1/2,1}}{\partial W_{(i,1)}}$$
$$+(\Lambda^T_{(i,1)}-\Lambda^T_{(i+1,1)})\frac{\partial F_{i+1/2,1}}{\partial W_{(i,1)}}+(\Lambda^T_{(i+1,1)}-\Lambda^T_{(i+2,1)})\frac{\partial F_{i+3/2,1}}{\partial W_{(i,1)}}$$
$$+(\Lambda^T_{(i,2)}-\Lambda^T_{(i,3)})\frac{\partial F_{i,5/2}}{\partial W_{(i,1)}}+(\Lambda^T_{(i,1)}-\Lambda^T_{(i,2)})\frac{\partial F_{i,3/2}}{\partial W_{(i,1)}}$$
$$-\Lambda^T_{(i,1)}\frac{\partial F_{i,1/2}}{\partial W_{(i,1)}}=-\frac{\partial J}{\partial W_{b_{(i,1/2)}}}\frac{\partial W_{b_{(i,1/2)}}}{\partial W_{(i,1)}} \quad (13)$$

For the two considered numerical fluxes it appears that outside zones of flow discontinuities the only first order terms in space in equation (13) are the last two terms. The characteritic space size is now denoted h and this property is briefly discussed in the case of Jameson-Schmidt-Turkel flux.[18] This numerical flux reads (omitting the j index)

$$\begin{aligned}F^{JST}_{i+1/2} &= (\mathbf{F}(W_i)+\mathbf{F}(W_{i+1})).S_{i+1/2}\\ &\quad -k_2\nu_{i+1/2}\rho_{i+1/2}(W_{i+1}-W_i)\\ &\quad +\overline{k_4}\rho_{i+1/2}(W_{i+2}-3W_{i+1}+3W_i-W_{i-1})\end{aligned}$$

with

$$\nu_i=\frac{|p_{i+1}-2p_i+p_{i-1}|}{(p_{i+1}+2p_i+p_{i-1})}$$
$$\nu_{i+1/2}=max(\nu_i,\nu_{i+1}) \qquad \overline{k_4}=max(0,k_4-\nu k_2)$$

where $\mathbf{F}$ is the Euler flux density tensor, $S_{i+1/2}$ the surface vector of the considered face, $\rho_{i+1/2}$ the spectral radius of the Jacobian of the finite-volume flux in the considered direction (including the edge length), k_2 and k_4 the second and fourth-order artificial coefficients. Note finaly that no artificial dissipation is involved in a physical boundary flux. Outside of shock-waves or slipping lines/planes, the derivative of the centred flux is well defined and is an $O(h)$ term. In regular zones, ν is an $O(h^2)$ term and deriving sensor, spectral radius and first order difference leads to $O(h^2)$ $O(h^4)$ and $O(h^3)$ terms. In regular zones, $\overline{k_4}$ is almost equal to k_4 and derivation of spectral radius and first order difference leads to $O(h^4)$ and $O(h)$ terms. In equation (13), the derivative of the inside fluxes are multiplied by the difference of the Λ of the two cells adjacent to the face so that the first five terms are $O(h^2)$ are lower in regular flow regions. The derivation of $F_{i,3/2}$ involves the ghost cell values $W_{j,0}=2W_{b(j,1/2)}-W_{(j,1)}$ but leads to the same conclusion. Finaly, outside of shock-waves or slipping lines/planes, only the last two terms of equation (13) are $O(h)$. Using the singular expression of Euler flux at a solid wall, fixing J as the pressure integral over the solid body projected in direction $\overline{d}$, the limit equality of the first order terms of (13) yields

$$-\Lambda^T_{(i,1)}\begin{pmatrix}0\\ Sx_{(i,1/2)}\\ Sy_{(i,1/2)}\\ 0\end{pmatrix}\frac{\partial p_{b_{(i,1/2)}}}{\partial W_{b_{(i,1/2)}}}\frac{\partial W_{b_{(i,1/2)}}}{\partial W_{(i,1)}}=$$
$$-\frac{\partial((-\overline{S_{(i,1/2)}}.\overline{d})p_{b_{(i,1/2)}})}{\partial W_{b_{(i,1/2)}}}\frac{\partial W_{b_{(i,1/2)}}}{\partial W_{(i,1)}}.$$

That is naturally simplified in

$$\Lambda^2_{(i,1)}Sx_{(i,1/2)}+\Lambda^3_{(i,1)}Sy_{(i,1/2)}+\overline{S_{(i,1/2)}}.\overline{d}=0 \quad \text{or}$$

or

$$\Lambda^2_{(i,1)}Sx_{(i,1/2)}+\Lambda^3_{(i,1)}Sy_{(i,1/2)}=-\overline{S_{(i,1/2)}}.\overline{d} \quad (14)$$

Equation (14) is obviously the cell-centred finite-volume counterpart of the continuous adjoint boundary condition at the wall (5). Please, note that it involves metric at the wall and adjoint at adjacent cell-centers and it has only been derived by equaling lower-order space terms in regular flow regions. How accurately equation (5) is satisfied is discussed for all test cases plotting together the purely geometric term ($-\overline{S_{(i,1/2)}}.\overline{d}$) and the adjoint term ($\Lambda^2_{(i,1)}Sx_{(i,1/2)}+\Lambda^3_{(i,1)}Sy_{(i,1/2)}$).

4 Drag and lift adjoint for inviscid flow about NACA0012 at M_∞=1.5 AoA=1^o

4.1 Flow solution

We first consider a supersonic flow calculation about the NACA0012 airfoil with a free-stream Mach number of M_∞ = 1.50 and an angle of attack AoA=1^o. According to the theory of supersonic flows about blunt bodies, the flow is supersonic and constant up to a detached shock-wave. Downstream the shock-wave, the flow is subsonic in a small bubble close to the airfoil leading edge and supersonic elsewhere. It accelerates along the airfoil up to a fishtail shock-wave based on the trailing edge. Downstream this second shock-wave the flow is still supersonic with a Mach number close to the upwind far-field Mach number – see figure 2.

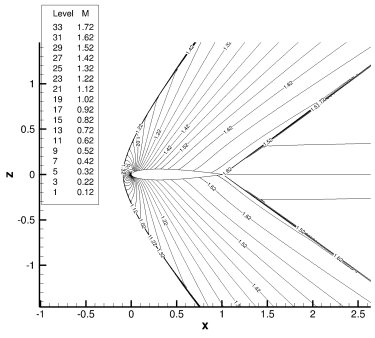

Figure 2: NACA0012 M_∞=1.50 AoA=1^o. 2049×2049 mesh –Iso-lines of Mach number

4.2 Lift and, drag adjoint fields. Mesh convergence and consistency

Discrete flows are converged to machine zero for all five considered structured meshes – 129×129 to 2049×2049 with the *elsA* code in steady state mode.[11] The partial derivatives of lift and drag with respect to flowfield are

calculated before the adjoint equations are solved by *elsA* adjoint module[22] for the two functions and the five meshes. The gradient of the discrete adjoint is then estimated at cell centers using Green formula and finally the residual of the continuous adjoint equation is evaluated:

$$res_{ij} = -A_{ij}^T \left(\frac{\partial \Lambda}{\partial x}\right)_{ij} - B_{ij}^T \left(\frac{\partial \Lambda}{\partial y}\right)_{ij}$$

(where A_{ij}^T and B_{ij}^T are the transposed Jacobians evaluated with cell-center values).
The percentage of cells with $|res|$ below a threshold is increasing as the mesh is refined. Nevertheless significant (and increasing) $|res|$ values are still observed on the finest meshes at the trailing edge and along the caracteristic lines starting from the trailing edge (where a perfect adjoint field would exhibit a discontinuity due to the end of the function support) – see figure 4.
Concerning far-field boundary conditions, the normal Mach number appears to be supersonic at the intersection of the characteristic geometrical strips (see far right plot in figure 6) and the far field boundary. No continuous adjoint boundary conditions is hence to be applied there and no check of discrete versus continuous adjoint is required.
Concerning the discrete equation (14) that is the counterpart of continuous boundary condition at the wall, its two terms are plotted in right part of figure (4.2). They appear to be superimposed so that equation (14) is actually satisfied.
As another mean to check the mesh convegence of adjoint fields, we have calculated the finest mesh adjoint-lift and adjoint-drag on another 2049 $\times$ 2049 mesh which J-mesh lines are streched close to the wall. The corresponding adjoint field can almost not be distinguished from the one obtained with the nominal mesh – see figure 4 This is an illustration of the intrisic nature of adjoint argumented by Giles and Pierce (§3).

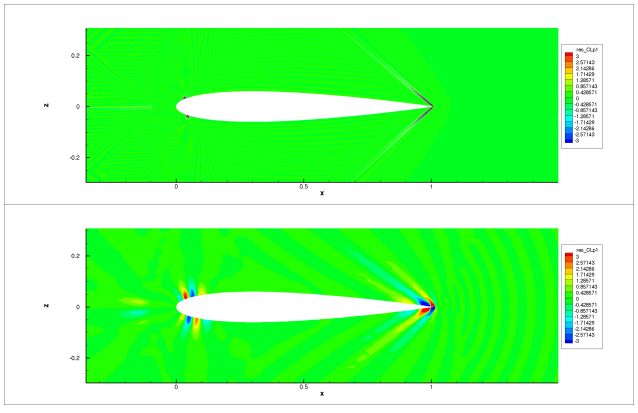

Figure 3: NACA0012 M_∞=1.50 AoA=1^o. down 129$\times$129 mesh, up 2049$\times$2049 mesh – Residual of the continuous equation (first component) evaluated with the discrete adjoint fields

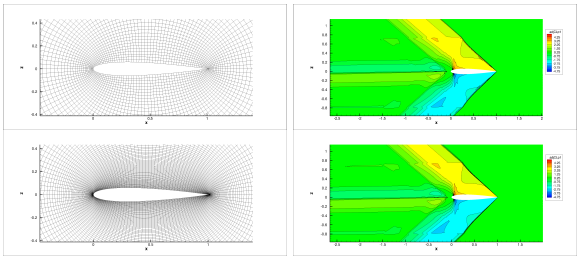

Figure 4: NACA0012 M_∞=1.50 AoA=1^o. aspect ratio of the two 2049$\times$2049 meshes (view of coarse extracted meshes with the same skip) – Corresponding first component of lift adjoint

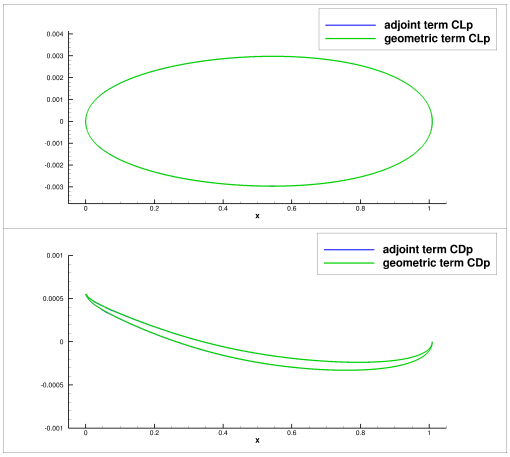

Figure 5: NACA0012 M_∞=1.50 AoA=1^o. Geometric and adjoint terms of equation (14) for lift and drag

4.3 *Analysis of adjoint field upwind the shock wave*

The inviscid continuous adjoint equation reads

$$-A^T \frac{\partial \lambda}{\partial x} - B^T \frac{\partial \lambda}{\partial y} = 0,$$

where A and B are the usual Jacobian matrices of Euler fluxes. The flow is supersonic and constant upwind the detached shock-wave so that A and B are constant matrices in this area. In a supersonic regime, Euler equations and adjoint-equation both exhibit specific directions of propagation corresponding to simple waves solutions,

$$\lambda(x,y) = \phi(x\sin(\gamma) - ycos(\gamma))\lambda_0,$$

where γ is the angle made by the direction of propagation with the x-axis, λ_0 is a vector representing the convected information and ϕ is a scalar function. Injecting this expression in the continuous adjoint equation yields

$$\phi'(x\sin(\gamma) - y\cos(\gamma)) \times (\sin(\gamma)A^T - cos(\gamma)B^T)\lambda_0 = 0.$$

This equation admits a non-trivial solution λ_0, if and only if

$$\det(\sin(\gamma)A^T - \cos(\gamma)B^T) = 0.$$

This condition is the same as the for supersonic Euler equations since the transposition plays no role in the calculation of the determinant. The eigenvalues of

$$(\sin(\gamma)A - cos(\gamma)B)^T$$

are: $(u_x\sin(\gamma) - u_y cos(\gamma)$, $u_x\sin(\gamma) - u_y\cos(\gamma) + c, u_x\sin(\gamma) - u_y cos(\gamma) - c)$. Since one of the eigenvalues is equal to 0, γ is solution of one of these equations:

$$\begin{aligned} u_x\sin(\gamma) - u_y\cos(\gamma) &= 0 \\ u_x\sin(\gamma) - u_y\cos(\gamma) + c &= 0 \\ u_x\sin(\gamma) - u_y\cos(\gamma) - c &= 0. \end{aligned}$$

AoA being the angle of incidence, the velocity components then read $u_x = ||V||\cos(\text{AoA})$ and $u_y = ||V||\sin(\text{AoA})$ Substituting these expressions yields

$$\begin{aligned} \gamma &= \text{AoA} \quad or \quad \text{AoA} + \pi \\ \gamma &= \text{AoA} - \alpha \quad or \quad \gamma = \text{AoA} - \alpha + \pi \\ \gamma &= \text{AoA} + \alpha \quad or \quad \gamma = \text{AoA} + \alpha + \pi \end{aligned}$$

where, α is the Mach angle: $\alpha = \arcsin(1/M_\infty)$. Hence, the information propagates along the three privileged directions $\gamma = \text{AoA}$, $\gamma = \text{AoA} - \alpha$ et $\gamma = \text{AoA} + \alpha$. Evidently, the domains of influence/dependance are inverse one another for state and adjoint variables.

The λ_0 eigenvectors of interest are those of $\sin(\gamma)A^T - \cos(\gamma)B^T$. These are also the left eigenvectors that appear in the more classical diagonalization of the inviscid flux Jacobian. Following,[23] the (left) eigenvector associated to $\gamma = \text{AoA} - \alpha$ is

$$\begin{pmatrix} \frac{-u_x n_x - u_y n_y}{2c} + \frac{(\gamma-1)V^2}{4c^2} \\ \frac{n_x c - (\gamma-1)u_x}{2c^2} \\ \frac{n_y c - (\gamma-1)u_y}{2c^2} \\ \frac{\gamma-1}{2c^2} \end{pmatrix}$$

The one associated to $\gamma = \text{AoA} + \alpha$ is

$$\begin{pmatrix} \frac{u_x n_x + u_y n_y}{2c} + \frac{(\gamma-1)V^2}{4c^2} \\ \frac{-n_x c - (\gamma-1)u_x}{2c^2} \\ \frac{-n_y c - (\gamma-1)u_y}{2c^2} \\ \frac{\gamma-1}{2c^2} \end{pmatrix}$$

The dimension of the eigenspace assciated to $\gamma = \text{AoA}$ is two but the classicaly exhibited left eigenvectors do not satisfy Giles and Pierce relation for pressure-based outputs ($\lambda_0^1 = H\lambda_0^4$). We search in this vector space the vectors that satisfy this relation and find $span(\lambda_0)$, λ_0 being

$$\begin{pmatrix} -1 - \frac{(\gamma-1)V^2}{2c^2} \\ \frac{(\gamma-1)u_x}{c^2} + \frac{2n_y}{n_y u_x - n_x u_y} \\ \frac{(\gamma-1)u_y}{c^2} - \frac{2n_x}{n_y u_x - n_x u_y} \\ -\frac{\gamma-1}{c^2} \end{pmatrix}$$

The finer the mesh, the better this propagation structure is actually observed – see figure 6. It has also been checked that the ratio of adjoint components inside each geometrical strip is equal to the ratio of the corresponding components of the associated λ_0 vector.

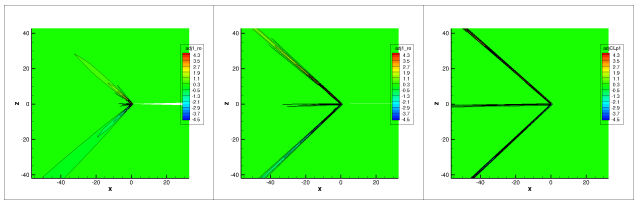

Figure 6: NACA0012 M_∞=1.50 AoA=1^o. far-field view of first component of CL_p adoint. 4097×4097 1025×1025 257×257 mesh

4.4 *Residual perturbation analysis in the supersonic zones*

The effect of residual perturbation that is observed with numerical steady state flows, closely follows the theoretical behaviour predicted by fluid dynamics: the influence is global in a subsonic zone and restricted to characteristic curves and trajectories in supersonic zones.[24] More precisely, in the later case [2]:

– δR^1 induces no change in the stagnation pressure,

[2] all variations are given for a positive ε in equation 10 and positive components of velocity for the nominal flow.

stagnation temperature, stagnation density and entropy. Mach number is decreased along the two characteristic lines starting from the pertubation location. The static pressure, temperature and density are increased and velocity components are also perturbed along these two lines with a decrease of velocity magnitude ;
– δR^2 induces no change in the stagnation pressure, stagnation temperature, stagnation density and entropy. Along the upper characteristic curve starting from the perturbation point, the static pressure, density, temperature, and y-component of velocity are increased whereas Mach number, velocity magnitude, x-component of velocity are decreased. Opposite variations are observed along the lower characteristic curve ;
– δR^3 induces no variation of stagnation pressure, static pressure, temperature and Mach number. An increase of total enthalpy, both components of velocity and entropy is observed along the trajectory starting from pertubation location. Also observed is a decrease of density ;
– δR^4 induces no variation of static pressure and total enthalpy. Mach number, density, stgnation density, and both velocity component are increased along the trajectory starting from pertubation location. Entropy and temperature are decreased compared along the trajectory.
The adjoint field is more complex to analyse downstream the shockwave where the flow is not constant. Nevertheless, the flow is supersonic everywhere but in a small bubble at the leading edge so that the zones influencing a specific point and the zones influenced by a perturbation at a given point follow essentialy the theory of characteristics. This explains in particular the aspect of (discrete) adjoint fields close to the trailing edge, that are bounded by two characterics curves starting from the trailing edge as seen in figure 8. This is also also illustrated in figure 7 by the influence of a δR^1 perturbation on the pressure field that is plotted together with the characteristic curves passing by the source location.
Finally, let us note that any perturbation in the small subsonic zone causes a noticeable change of the flow in all the neighborhood of the location of the source term. This is consistent with information propagation theory for subsonic flows.

4.5 *Discontinuity of adjoint derivatives at shockwaves*

It is known adjoint variables are continuous at shock-waves whereas, for Euler flows, their derivatives are possibly discontinuous.[3,9] In the fine grid numerical simulations, a clear discontinuity of the adjoint-drag or the adjoint-lift gradient is observed for the adjoint component associated to z-coordinate momentum equation– see figure 8. The compatibility of this gradient discontinuity with the continuous adjoint jump relations[9] is currently under investigation.

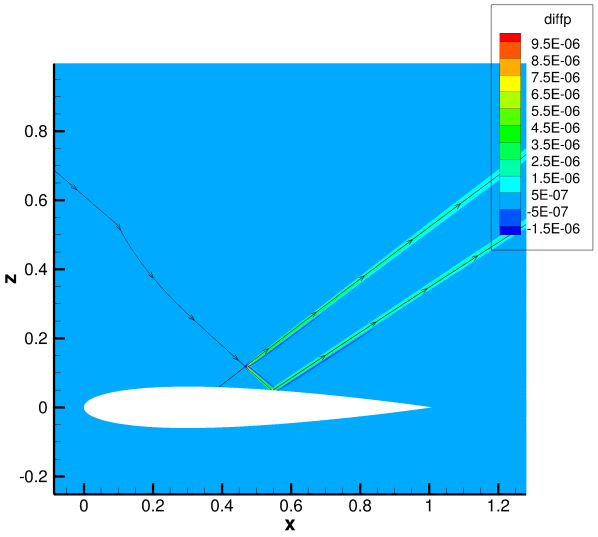

Figure 7: NACA0012 M_∞=1.50 AoA=1^o. 2049×2049 mesh. Residual perturbation δR^1_m

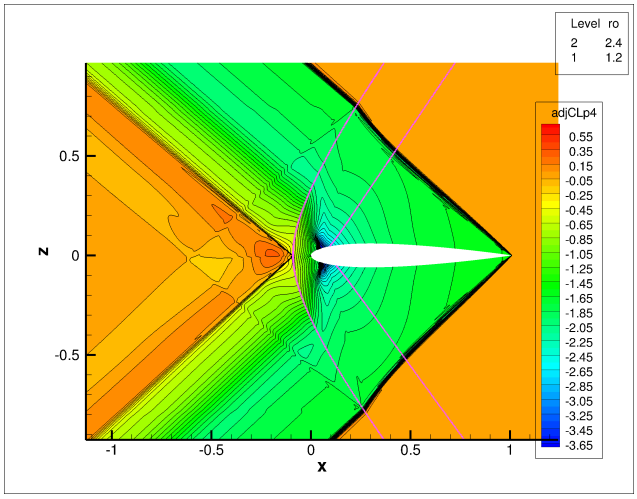

Figure 8: NACA0012 M_∞=1.50 AoA=1^o. 2049×2049 mesh –Iso-lines of adjoint component associated to z-coordinate momentum equation. Upwind pink line located at the shock-wave

5 Drag and lift adjoint for inviscid flow about NACA0012 at M_∞=0.85 AoA=2^o

5.1 Flow solution

This is classical transonic lifting case with a strong shock-wave on the suction side and a weaker shock on the pressure side (the Mach number upwind the shock at the wall respectively being roughly 1.5 and 1.2). Iso-Mach number iso-lines are presented by figure 9 whereas figure 10 presents the location of points for residual perturbation analysis.

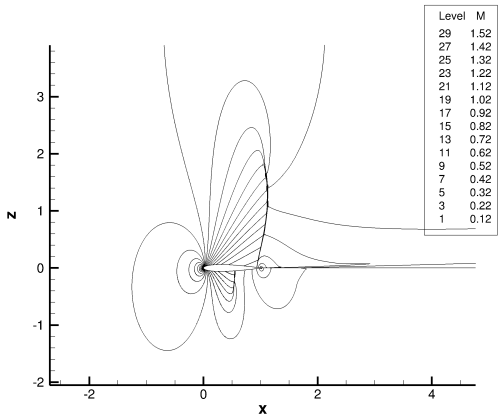

Figure 9: NACA0012 M_∞=0.85 AoA=2^o. 2049×2049 mesh –Iso-lines of Mach number

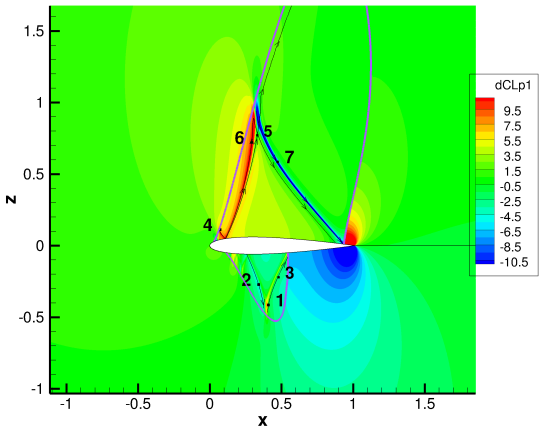

Figure 10: NACA0012 M_∞=0.85 AoA=2^o. 2049×2049 mesh. Location of points for the residual perturbation analysis

5.2 Lift and drag adjoint. Mesh convergence and consistency

The residual of the continuous adjoint equation is calculated as detailed in (§4.2). As the mesh is refined the zones with significant residual have a decreasing area but high and increasing values are observed close to the wall, the stagnation streamline and the caracteristic line that impacts the upperside shock foot, that are known to be zones of high values and gradient for the adjoint of lift and drag[8,9,25] – see figure 10. The far-field adjoint boundary condition is satisfied by the discrete adjoint fields as the adjoint field is almost null at the far-field boundary. Figure 5.2 illustrates the verification of continuous-like adjoint wall boundary condition ; equation (14) is actually satisfied execept at shock feet and trailing edge, where difference in neighboring λ terms are too big for a simple main-order in space analysis.

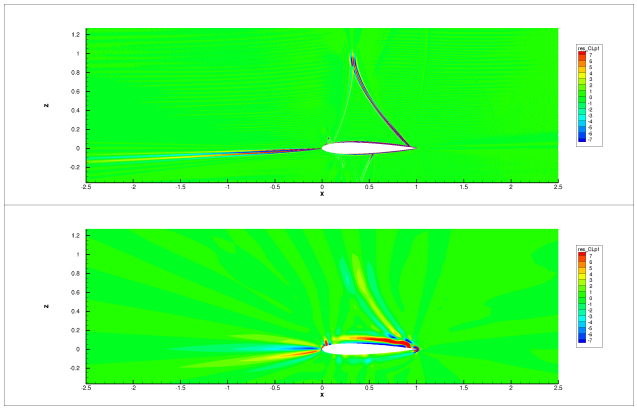

Figure 11: NACA0012 M_∞=0.85 AoA=2^o. down 129×129 mesh, up 2049×2049 mesh – Residual of continuous equation residual (first component) evaluated with the discrete adjoint fields

5.3 Residual perturbation analysis

The first order variation of CL_p and CD_p in response to the physical δR perturbations – equations (10) and (8) – are calculated. More precisely, the ε is removed from equation (10) and the intensity of δJ is calculated by equation (8) and affected in the plot to the source term location.

The δR^3 perturbation has no influence on the pressure field as discussed before.

The δR^1 and δR^2 perturbations lead to δCLp^1 and $\delta CLp2$ (respectively δCDp^1 and δCDp^2) exhibiting strong (positive and negative) values along two characteristic lines of the supersonic areas upwind the upper-side and lower side shock-waves. In order to search the reason of this, the flow perturbation δW due to the δR^1 and δR^2 source terms are calculated [3] for sources located at points 4, 5,

[3] with ε fixed to $6.e-6$, the infinite density, and velocity magnitude being used to render the Euler equations dimensionless

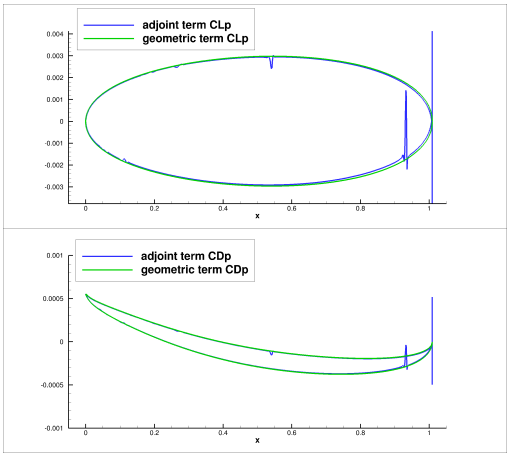

Figure 12: NACA0012 M_∞=0.85 AoA=2^o. Geometric and adjoint terms of equation (14) for lift and drag (2049×2049 mesh)

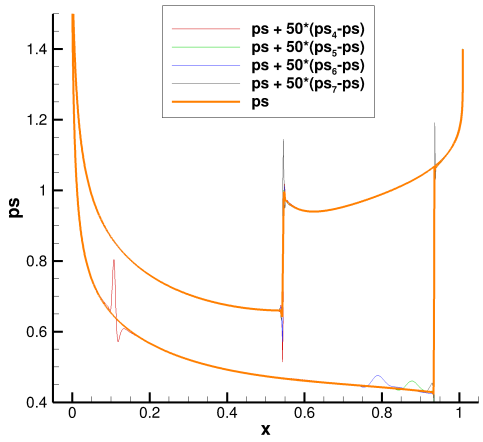

Figure 13: NACA0012 M_∞=0.85 AoA=2^o. 2049×2049 mesh – Pressure at the wall. (50 times amplified) influence of δR^1 source term located at points 5, 6, 7 and 8

6 and 7. The changes in the wall pressure field (of the reconverged flow) due to δR^1 source terms are illustrated in figure 13. The zones of the wall where changes in static pressure are the cause of the notable variations of CLp and CDp are analyzed. They are detailed for CLp and δR^1: for a source term located at point 4, there is a visible local oscillation of the pressure at about $x = 0.15$ but the change in CLp is due to global variations of static pressure all along the airfoil. For point 6, the change in CLp is due to displacement of the lower-side shock-wave and variation in pressure where the lower characteristic passing at point 6 impacts the wall (small bump at $x \simeq 0.78$, upperside, in figure 13). Concerning point 7, the change in CLp is due to displacement of both, upperside and lower-side shock-waves. Point 5 has been placed close to point 6 and 7 in order to better understand why a point close to the two well-marked characteristic curves may have a weak influence on CLp and CDp. Actually for this point, the influence upper side shock-wave displacement and lower characteristic impact (small bump at $x \simeq 0.87$, upperside, in figure 13) almost cancel and explain the low influence on lift (and hence the low δCLp^1 value).

5.4 Discontinuity of adjoint derivatives at shockwaves

As recalled before, adjoint variables are continuous at shock-waves whereas, for inviscid flows, their derivatives may be discontinuous.[3,9] In the fine grid numerical solutions, for this transonic flow, a clear discontinuity of the gradient of the drag or the lift adjoint is observed for the adjoint component associated to z-coordinate momentum equation – see figure 14. Whether the derivatives satisfy the continuous adjoint jump relations is currently investigated.

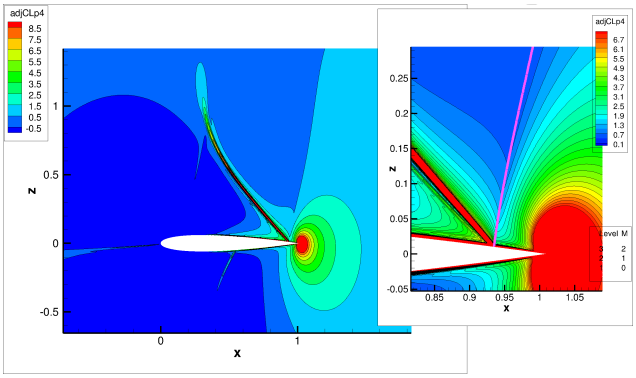

Figure 14: NACA0012 M_∞=0.85 AoA=2^o. 2049×2049 mesh –Iso-lines of adjoint component associated to z-coordinate momentum equation. Pink line located at the shock-wave

6 Conclusion

Researches are ongoing at ONERA about open theoretical questions related to adjoint fields. The study is based on 2D inviscid flows calculated on very fine meshes and corresponding lift and drag discrete adjoint computations. The consistency of the discrete adjoint fields with the continuous adjoint equation in the fluid domain is first checked. It is actually satisfactory for the considered flows. The consistency with farfield boundary condition is observed. The link established by Giles and Pierce[3] between density-equation adjoint and energy-equation adjoint is also satisfied. Besides, for the supersonic test case, a specific analysis has been carried out : the continuous lift drag adjoint fields, upwind the detached shock-wave, appear to be the sum of three simple waves and the numerical adjoint fields match more and more closely with this property as the mesh is refined.
The considered transonic and supersonic flows both include at least one shock-wave. At this location, a clear discontinuity of adjoint gradient is observed for the momentum-equation adjoint. The consistency between the numerical solutions and the continuous adjoint jump relations[9] is currently investigated.
The oral presentation of this research will also include the corresponding analysis for two other flow conditions, (M_∞,AoA)= (0.40,5) and (0.95,0).

References

[1] Anderson, W. and Bonhaus, D. Airfoil design optimization on unstructured grids for turbulent flows. *AIAA Journal* **37**(2), 185–191 (1999).

[2] Nielsen, E. and Anderson, W. Aerodynamic design optimization on unstructured meshes using the Navier-Stokes equations. *AIAA Journal* **37**(11), 185–191 (1999).

[3] Giles, M. and Pierce, N. Adjoint equations in CFD: Duality, boundary conditions and solution behaviour. In *AIAA Paper Series, Paper 97-1850*. (1997).

[4] Peter, J. and Dwight, R. Numerical sensitivity analysis for aerodynamic optimization: a survey of approaches. *Computers and Fluids* **39**, 373–391 (2010).

[5] Hicken, J. and Zing, D. Dual consistency and functional accuracy: a finite-fdifference perspective. *Journal of Computational Physics* **256**, 161–182 (2014).

[6] Stück, A. An adjoint view on flux consistency and strong wall boundary consditions to the navier stokes equations. *Journal of Computational Physics* **301**, 247–264 (2015).

[7] Lozano, C. A note on the dual consistency of the discrete adjoint quasi-one dimensional Euler equations with cell-centred and cell-vertex central discretization. *Computers and Fluids* **134-135**, 51–60 (2016).

[8] Lozano, C. On the properties of the solutions of the 2D adjoint Euler equations. In *Proceedings of EUROGEN 2017, Madrid*, (2017).

[9] Lozano, C. Singular and discontinuous solutions of the adjoint Euler equations. *AIAA Journal* **56**(11), 4437–4451 (2018).

[10] Vassberg, J. and Jameson, A. In pursuit of grid convergence for two-dimensional Euler solutions. *Journal of Aircraft* **47**(4), 1152–1166 (2010).

[11] Cambier, L., Heib, S., and S., P. The elsA CFD software: input from research and feedback from industry. *Mechanics & Industry* **14**(3), 159–174 (2013).

[12] Jameson, A. Aerodynamic design via control theory. *Journal of Scientific Computing* **3**(3), 233–260 (1988).

[13] Giles, M. and Pierce, N. An introduction to the adjoint approach to design. In *Proceedings of ERCOFTAC Workshop on Adjoint Methods*, (1999).

[14] Giles, M. and Pierce, N. An introduction to the adjoint approach to design. *Flow, Turbulence, Combustion* **65**, 393–415 (2000).

[15] Anderson, W. and Venkatakrishnan, V. Aerodynamic design optimization on unstructured grids with a continuous adjoint formulation. *Computers and Fluids* **28**, 443–480 (1999).

[16] Hiernaux, S. and Essers, J.-A. An optimal control theory based algorithm to solve 2D aerodynamic shape optimisation problems for inviscid and viscous flows. In *Proceedings of the RTO-AVT Symposium on Aerodynamic Design and Optimisation of Flight Vehicles*, (1999).

[17] Hiernaux, S. and Hessers, J.-A. Aerodynamic optimization using Navier-Stokes equations and optimal control theory. In *AIAA Paper Series, Paper 99-3297*. (1999).

[18] Jameson, A., Schmidt, W., and Turkel, E. Numerical solutions of the Euler equations by finite volume methods using Runge-Kutta time-stepping schemes. In *AIAA Paper Series, Paper 1981-1259*. (1981).

[19] Roe, P. Approximate Riemann solvers, parameters vectors, and difference schemes. *Journal of Computational Physics* **43**, 292–306 (1983).

[20] van Leer B. Towards the ultimate conservative difference scheme. V – a second order sequel to Godunov's method. *Journal of Computational Physics* **32**, 101–136 (1979).

[21] van Albada, G., van Leer, B., and Robers Jr, W. A comparative study of computational methods in cosmis gas dynamics. *Astronomy and Astrophysics* **108**, 76–84 (1982).

[22] Peter, J., Renac, F., Dumont, A., and Méheut, M. Discrete adjoint method for shape optimization and mesh adaptation in the *elsA* code. Status and challenges. In *Proceedings of 50th 3AF Symposium on Applied Aerodynamics, Toulouse*, (2015).

[23] Jameson, A. Eigenvalues and eigenvectors for the gas dynamic equations. Technical report, Stanford University, April (2001).

[24] Délery, J. *Traité d'aérodynamique compressible. Volume 3*. Collection mécanique des fluides. Lavoisier, (2008).

[25] Todarello, G., Vonck, F., Bourasseau, S., Peter, J., and Désidéri, J.-A. Finite-volume goal-oriented mesh-adaptation using functional derivative with respect to nodal coordinates. *Journal of Computational Physics* **313**, 799–819 (2016).

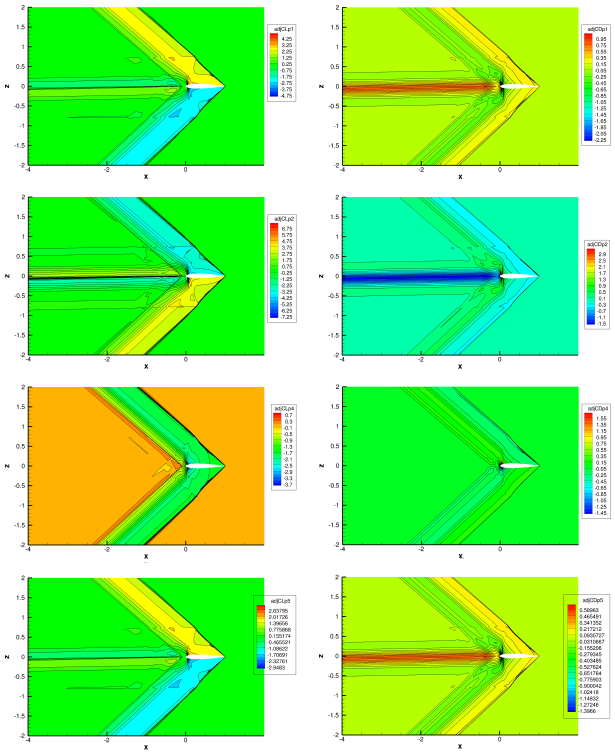

Figure 15: NACA0012 M_∞=1.50 AoA=1^o inviscid flow. 2049×2049 mesh – Left: lift adjoint. Right: drag adjoint

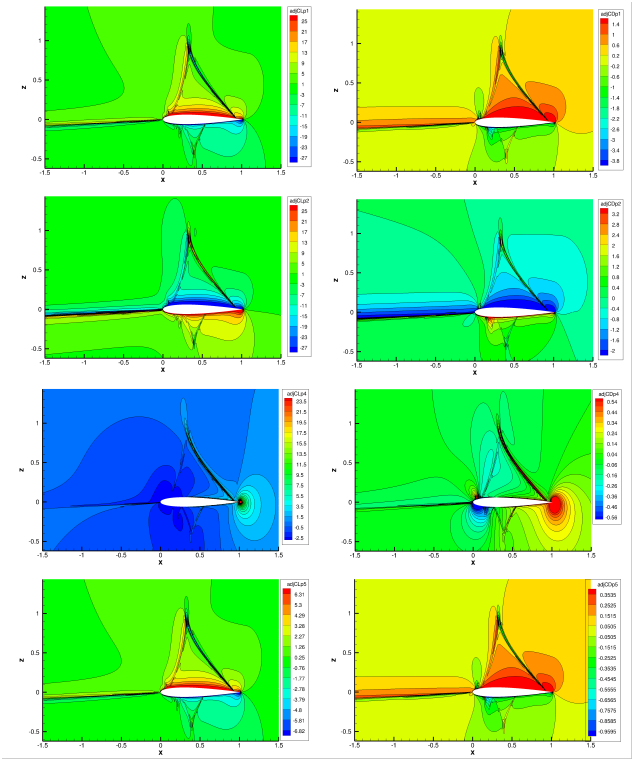

Figure 16: NACA0012 M_∞=0.85 AoA=2^o inviscid flow. 2049×2049 mesh – Left: lift adjoint. Right: drag adjoint